Factors Governing the Enhancement of Hydrocarbon Recovery via H_2S and/or CO_2 Injection: Insights from a Molecular Dynamics Study in Dry Nano-Pores

Sakiru B. Badmos, Tai Bui, and Alberto Striolo*

Department of Chemical Engineering
University College London
London, WC1E 7JE, UK

David R. Cole

School of Earth Sciences
The Ohio State University
Columbus, Ohio 43210, USA

ABSTRACT

Although enhanced oil recovery (EOR) is often achieved by CO_2 injection, the use of acid gases has also been attempted, for example in oil fields in west Canada. To design EOR technologies effectively, it would be beneficial to quantify the molecular mechanisms responsible for enhanced recovery under various conditions. We report here molecular dynamics simulation results that probe the potential of recovering *n*-butane confined from silica, muscovite and magnesium oxide nano-pores, all proxies for subsurface materials. The three model solid substrates allow us to identify different molecular mechanisms that control confined fluid behavior, and to identify the conditions at which different acid gas formulations are promising. The acid gases considered are CO_2, H_2S, as well as their mixtures. For comparison, in some cases we consider the presence of inert gases such as N_2. In all cases, the nano-pores are dry. The recovery is quantified in terms of the amount of *n*-butane displaced from the pore surface as a function of amount of gases present in the pores. The results show that the gas performance depends on the chemistry of the confining substrate. While CO_2 is more effective at displacing *n*-butane from the protonated silica pore surface, H_2S is more effective in muscovite, and both gases show similar performance in MgO. Analysis of the interaction energies between the confined fluid molecules and the surface demonstrates that the performance depends on the gas interaction with the surface, which suggests experimental approaches that could be used to formulate the gas mixtures for EOR applications. The structure of the gas films at contact with the solid substrates is also quantified, as well as the self-diffusion coefficient of the fluid species in confinement. The results could contribute to designing strategies for achieving both improved hydrocarbon production and acid gas sequestration.

Keywords: Preferential adsorption, Structure-transport relation, Adsorption

* Corresponding Author: a.striolo@ucl.ac.uk

1.0 INTRODUCTION

The growing concern about greenhouse gas emissions has stimulated research into developing new technologies for capturing and sequestering CO_2. CO_2 injection into geological formations has received much attention,[1-8] sometimes as a long-term storage opportunity, while in some other cases CO_2 has been injected in oil and gas fields to attempt to simultaneously achieve enhanced hydrocarbon recovery and CO_2 sequestration.[9] For these strategies to be fully optimised, it is important to understand, and ultimately control the molecular mechanisms that are responsible for rock-fluid interactions, inclusive of fluid sorption, migration, and fixation.[10]

We consider here enhanced oil recovery (EOR). EOR methods commonly used include water, gas, and surfactant injection.[11-14] The technology follows either the flooding or the huff-n-puff mode. The huff-n-puff mode is sometimes preferred for shale formations due to their ultra-low permeability, which delays gas and pressure propagation from the injector to the producer well.[15] It has been reported that waterflooding can yield much lower recovery compared to gas injection, which sometimes justifies the use of gas injection as the preferred option.[16]

Several studies have been reported in the literature concerning efforts directed towards understanding the mechanisms responsible for CO_2–based EOR.[7-8, 14, 17-23] In general, the enhancement of hydrocarbon recovery is either attributed to preferential adsorption of CO_2 on the pore surfaces, [8, 24-26] or the dissolution of CO_2 in oil, which swells the oil and reduces its viscosity.[6, 27-29] Previous research from our group[24] reported that CO_2 preferentially adsorbs on silica surfaces, weakening *n*-butane adsorption, and effectively acting as a 'molecular lubricant' that lowers the activation energy for *n*-butane diffusion. Santos et al.[21] conducted molecular dynamics simulations in slit-shaped calcite pores to study the effect of CO_2 on *n*-alkanes displacement. They identified several factors that control the preferential adsorption of CO_2 on calcite, including the amount of CO_2 present, temperature, hydrocarbon length, and pore size. Wang et al.[22] observed an increase in *n*-decane diffusion as CO_2 loading increases, and reported a maximum diffusion due to pore crowding.

Experimental studies on CO_2 – based EOR are also common.[30-33] Jin et al.[30] carried out experimental studies on core samples from the Bakken shale formation, and found that supercritical CO_2 injection

facilitates the recovery of up to 65% of hydrocarbons in place; they also reported that CO_2 is trapped in the reservoir over a wide pressure range. Eide et al.[31] reported experimental results on oil recovery by CO_2 injection into fractured core sample using nuclear magnetic resonance (NMR) and X-ray computed tomography; they reported oil recovery in excess of 90% of the original oil in place.

Current research focuses on coupling EOR with CO_2 sequestration. However, sequestering H_2S resulting from oil and gas processing into geological formations is also desirable, and could lead to EOR. Acid gases (CO_2+H_2S) have been injected into geological formations to reduce atmospheric emissions and at the same time enhance hydrocarbon recovery.[34] Field tests have been reported where acid gases were injected into geological formations in the Alberta basin of western Canada.[35] However, Khan et al.[34] performed reservoir simulation studies complemented by experimental data from Clean Gas Technology Australia (CGTA) as input; based on those reservoir simulations, injecting a mixture of CO_2 and H_2S yields a lower recovery factor compared to injecting pure CO_2.

Because it is possible that the performance of an EOR strategy depends on the formation features (rocks, pressure, temperature, hydrocarbons in place, porosity, presence of other fluids such as water, etc.), a detailed molecular-level understanding of the mechanisms responsible for EOR is desirable. This could be achieved by extensive molecular simulations. While results have been reported for CO_2, CH_4 and other hydrocarbons in nanopores, few studies explicitly attempted to quantify the behaviour of H_2S and its mixtures with CO_2 within narrow pores.[36] An exception is our recent study,[37] where we reported that H_2S solubility in water confined in narrow pores is much lower compared to the H_2S solubility in bulk water because confinement in nano-pores can strongly affect the hydration shell of aqueous H_2S.

In this manuscript, we investigate the *n*-butane displacement due to pure H_2S, pure CO_2 as well as their mixtures within slit-shaped nano-pores carved out of silica, muscovite, and magnesium oxide (MgO). The three pores are chosen because silica and muscovite are considered representative of many sub-surface formations, while MgO is a model substrate useful for quantifying the molecular phenomena responsible for the results obtained. It should be noted that the MgO surface considered here is not hydroxylated. As such, our system provides a model surface useful for understanding the molecular driving forces at play for the systems considered, but it does not provide a good model for real

substrates, e.g. brucite. Because the systems considered here are dry, pH effects on the pore surfaces are not described. An exception is the silica substrate, which is protonated in our model. Certainly, the presence of water would affect the results presented, and future studies, conducted perhaps with reactive force fields, should address such effects. We focus on the molecular behaviour of the fluids at the solid-fluid interface, as well as the transport of the confined fluids. We employ the method of atomistic molecular dynamics (MD) simulations to probe the effect of molecular interactions on the results obtained. While EOR performance cannot be directly quantified by the MD approach implemented here, the results are analysed in terms of the preferential adsorption of *n*-butane vs. acid gases on the solid surfaces. The implicit assumption is that the dislocation of *n*-butane from the proximity to the solid substrates promotes EOR.

The remainder of this manuscript is organized as follows: in Section 2 we describe the simulation models and algorithms implemented in this study; in Section 3 we present the simulation results; we then conclude by briefly discussing and summarizing our main findings.

2 SIMULATION MODELS AND METHODOLOGY

2.1 Simulation set up

Molecular dynamics (MD) simulations were conducted for binary and ternary fluid systems composed of systems of C_4H_{10}-H_2S, C_4H_{10}-CO_2, C_4H_{10}-N_2 and C_4H_{10}-H_2S-CO_2 at various compositions confined within slit-shaped pores of width 22Å carved out of silica, muscovite, and MgO. These substrates are representative of many minerals or mineral components found in sub-surface formations. The silica surface was obtained by cutting β-cristobalite crystal along the (1,1,1) crystallographic plane; the non-bridging oxygen atoms were fully protonated yielding a reasonable proxy for hydrophilic surfaces.[38] The resulting –OH surface density is 4.54 per square nanometer. The model MgO slab was obtained from the space group Fm3m replicated along the (001) plane.[39-40] The exposed MgO surface was not hydroxylated in our model. While this model is not realistic, it allows us to quantify the mechanisms responsible for preferential adsorption. Muscovite was considered a model for clays, used in our prior investigations. Details regarding this substrate are available elsewhere.[41-43] Muscovite is a phyllosilicate

mineral with structure similar to illite.[44] In muscovite, an interlayer of potassium ions holds a Tetrahedral-Octahedral-Tetrahedral (T-O-T) structure of Al-centred octahedral sheets sandwiched between two Si-centred tetrahedral sheets in which one Al atom substitutes one out of every four Si atoms. The potassium ion-bearing interlayer balances the negative charge and holds the T-O-T layers via electrostatic interactions.[41] Each octahedral sheet contains two oppositely pointing –OH groups. The surface of each muscovite slab is not protonated in our studies, but it contains potassium ions resulting from cleavage along its basal plane (001). Muscovite with this surface termination has been used in several studies.[41-43, 45-47] No water is considered in the present study, although it would certainly affect the results, for example via the solvation of the K^+ ions.

All solid substrates simulated bear no net charge and were kept rigid throughout the simulation. Exceptions were the surface hydrogen atoms in silica and potassium ions on muscovite, which were allowed to vibrate. Each solid slab was maintained parallel to the X-Y plane of the simulation box. The X and Y dimensions for the three systems were 51.7 x 100.8, 47.2 x 73.4, and 47.2 x 73.6 $Å^2$ for silica, muscovite and MgO, respectively. The Z dimension of the simulation box was set to 54.92, 58.30 and 53.52 Å for silica, muscovite, and MgO, respectively. These dimensions yield slit-shaped pores 22Å wide, measured as the shortest centre-to-centre distance between the oxygen atoms of the –OH groups on silica slabs, surface potassium ions in muscovite slabs and surface magnesium atoms in MgO across the pore volume. Because periodic boundary conditions (PBC) were applied in all directions, the simulated systems are infinitely long in X and Y directions.

The pores were loaded with 300 molecules of n-butane. It is estimated that this amount of hydrocarbon corresponds to approximately 60% of the maximum loading in silica pores at 350K. We report in **Supporting Information** details regarding these simulations, and the maximum amount of n-butane, CO_2 and H_2S estimated to be confined within the pores used int his work at moderate pressures.

Binary systems containing *n*-butane and H_2S were simulated at different compositions: 300 molecules of *n*-butane were diluted with H_2S at different loadings. These are systems 1-3 in **Table 1**. Note that the number of *n*-butane molecules is maintained constant for all these simulations. Snapshots for *n*-butane-H_2S systems for the maximum H_2S loading are shown in **Figure 1**.

Binary systems containing *n*-butane-CO_2 and *n*-butane-N_2 were also simulated at different compositions: 300 molecules of *n*-butane were diluted with CO_2 and with N_2 at different loadings. These are systems 4-6 and 7-9, respectively, in **Table 1**. Representative snapshots for *n*-butane-CO_2 and *n*-butane-N_2 systems confined in the three pores are shown in **Supporting Information** (SI).

To study the effect of H_2S-CO_2 mixtures and the presence of an inert gas (nitrogen) on the displacement of *n*-butane from the pore surface, we simulated ternary systems of *n*-butane-H_2S-CO_2 with varying compositions of the acid gases. These are systems 10-12 in **Table 1**. *n*-butane-acid gas-nitrogen (N_2) systems are identified as 13-16 in **Table 1**.

As the system composition and the amount of fluid molecules confined in the pores change, so does the pressure. To relate the system composition to bulk pressure, we performed simulations in which the pores are in contact with bulk reservoirs. Constraining the number of n-butane in the pores, CO_2 and H_2S molecules were allowed to exchange between the pores and the reservoirs. The bulk pressure was calculated from the density in the reservoirs, as explained in the Supporting Information (Figure S1). In **Table 2** we report the pressure ranges corresponding to the systems summarised in **Table 1**. Pressures for muscovite and MgO pores were similar, while silica pores were at somewhat lower pressures.

Table 1: Composition of all systems simulated in this work.

System	Number of *n*-butane	Number of H_2S	Number of CO_2	Number of N_2
1	300	200	-	-
2		375	-	-
3		500	-	-
4		-	200	-
5		-	375	-
6		-	500	-
7		-	-	300
8		-	-	500
9		-	-	700
10		250	250	-
11		125	250	-
12		250	125	-
13		400	-	100
14		300	-	200
15			400	100
16			300	200

Table 2: Bulk Pressures corresponding to the systems summarised in Table 1. For each pore, we report the lower and upper pressures, as estimated at increasing acid gas loading. For details, please refer to Figure S1 of the SI.

Substrate	**Pressure / MPa (n-butane with_H_2S)**	**Pressure / MPa (n-butane with_CO_2)**
Silica	14.2 ± 0.2 – 7.8 ± 0.3	14.0 ± 0.2 – 7.6 ± 0.3
Muscovite	21.0 ± 0.2 – 11.2 ± 0.2	19.2 ± 0.1 – 10.9 ± 0.2
MgO	23.2 ± 0.2 – 12.1 ± 0.3	20.1 ± 0.1 – 11.2 ± 0.2

2.2 Force fields

The CLAYFF force field was implemented to model silica, muscovite, and MgO.[48] *n*-Butane, and CO_2 were modeled using the TraPPE-UA force field.[49] In TraPPE-UA, CO_2 is rigid with all atoms on a straight line forming a bond angle of 180°. *n*-Butane is flexible, described by bond stretching, angle bending and dihedrals. The united-atom formalism was implemented to describe -CH_3 and -CH_2 groups of *n*-butane. H_2S was described by the model developed by Kamath and Potoff.[50] Nitrogen (N_2) was described as a single LJ sphere without Coulombic interactions.[51] The N_2 model implemented here was found to reasonably reproduce the experimental adsorption isotherm of N_2 in silica pores.[51] In all cases, non-bonded interactions were modeled by dispersive and electrostatic interactions. The electrostatic interactions were modeled by Coulombic potential and the dispersive interactions were described by 12-6 Lennard-Jones (LJ) potentials. The LJ parameters for unlike atoms were obtained using Lorenz-Berthelot combination rules.[52] The cut-off distance for all interactions was set to 14Å. The particle mesh Ewald method was implemented for long-range corrections to electrostatic interactions.[53]

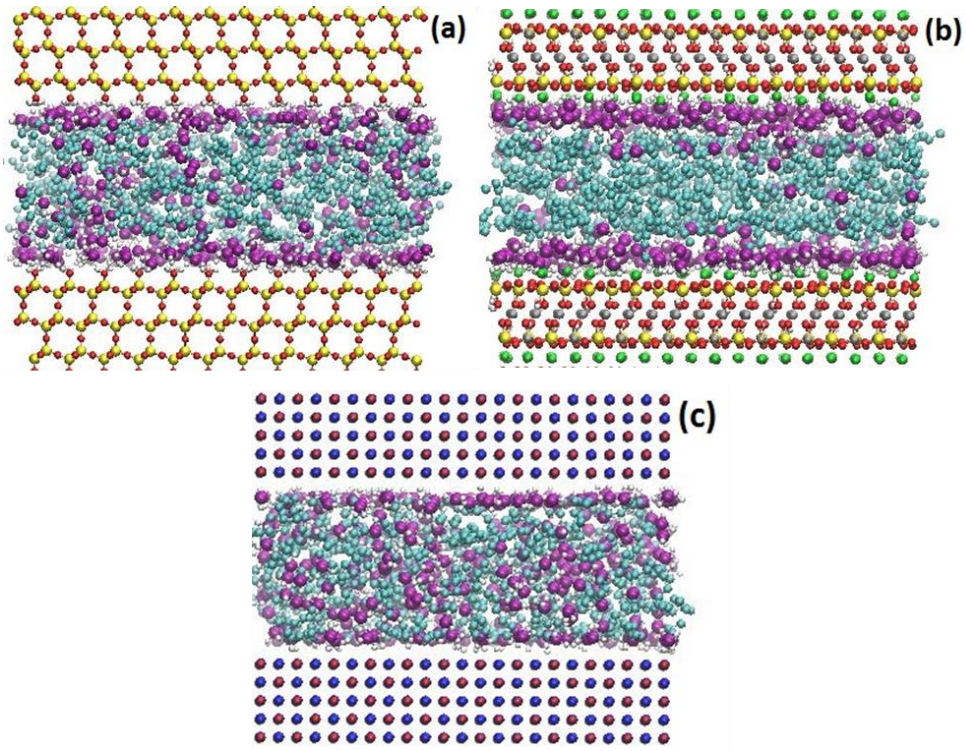

Figure 1: Simulation snapshots for binary systems containing *n*-butane and H_2S in silica (a) MgO (b) and muscovite (c). All systems shown contain 300 *n*-butane and 500 H_2S molecules. Cyan spheres are $-CH_3$ and $-CH_2$ in *n*-butane, purple are sulphur, white are hydrogen, red are oxygen, yellow are silicon, green are potassium, grey are aluminium, blue are magnesium. For clarity, only a portion of the solid substrates are shown along the Z direction. Please refer to Section 2.1 for details regarding the size of the simulation boxes.

2.3 Algorithms

All simulations were performed within the canonical ensemble, in which the number of molecules, volume, and temperature were maintained constant (NVT). The simulation package GROMACS, version 5.1.2,[54-55] was used for conducting the simulations. Numerical integration of Newton's equations of motion was performed using the leapfrog algorithm with a time step of 1fs. The temperature of the solid substrates and of the fluid molecules were controlled separately using two Nosé-Hoover thermostats with relaxation times of 200fs. The simulations were conducted at 350K, a temperature representative of depths between 11,000 and 15,000 feet in sub-surface formations. The total simulation time for each system was in the range of 60-80 ns, depending on the system and the loading. The system was considered equilibrated when *n*-butane and acid gas densities fluctuated around a constant value, and the system energy fluctuated within 10% of the average values. In Figure

S2 of the SI we report representative data for the interaction energy as a function of simulation time for the systems considered here. The results confirm that equilibration was achieved. The production phase was conducted at the end of the simulations, and data analysis was conducted over the last 10 ns of each simulation.

3 RESULTS AND DISCUSSION

3.1 Binary Systems: Enhancement of Butane Displacement by H_2S and CO_2 in Silica Pores

3.1.1 Density profiles

The distribution of fluid molecules in the pore is quantified in terms of the molecular density profiles along the direction perpendicular to the pore surface. The density profiles calculated for the centre of mass (COM) of *n*-butane at different H_2S, CO_2 and N_2 loadings are shown in **Figure 2.** The density profile results show preferential adsorption of *n*-butane on the pore surfaces, as evidenced by the high peak density. The height of the *n*-butane density peak closest to the solid substrate reduces as the H_2S density is increased, suggesting that the amount of *n*-butane in contact with the pore surface decreases. The results show that adding CO_2 also reduces the intensity of the density peak closest to the solid substrate. Conversely, adding N_2 leaves the density profile relatively unchanged, as discussed shortly.

The density profiles of the hydrogen and sulphur atoms of H_2S, of the carbon and oxygen atoms of CO_2, and of N atom of N_2 in the binary systems considered in **Figure 2** are shown in **Figure 3**. The distribution of H_2S in the pore is similar to that of CO_2 in the binary systems. At low loading, most of the H_2S and CO_2 in the pore are adsorbed close to the pore surface while at higher loadings, some H_2S and CO_2 molecules occupy regions close to the pore centre, as the pore surface becomes more saturated.

To quantify these results, we calculated the percentage of *n*-butane displaced from the first adsorbed layer (FAL) by:

$$\eta_{displaced} = \frac{\left(N_{initial} - N_{gas}\right)}{N_{initial}} \quad (1)$$

In Eq. (1), $N_{initial}$ and N_{gas} represent the amount of *n*-butane in the FAL in the system without acid gas and with acid gas respectively. $\eta_{displaced}$ is calculated within the narrow region confined between the

position of the first peak in *n*-butane COM density profile and the pore surface. The results, obtained from the density profiles, are shown in **Table 3** and confirm that both CO_2 and H_2S aid displacing *n*-butane from the pore surfaces. It appears that CO_2 is slightly more effective than H_2S.

Table 3: Percentage of *n*-butane displaced with H_2S and CO_2 loading. Uncertainties, estimated by block averaging the simulation results, are ~ 1 in all cases.

Loading	% displaced (H_2S loading)	% displaced (CO_2 loading)
200	28	34
375	48	55
500	58	65

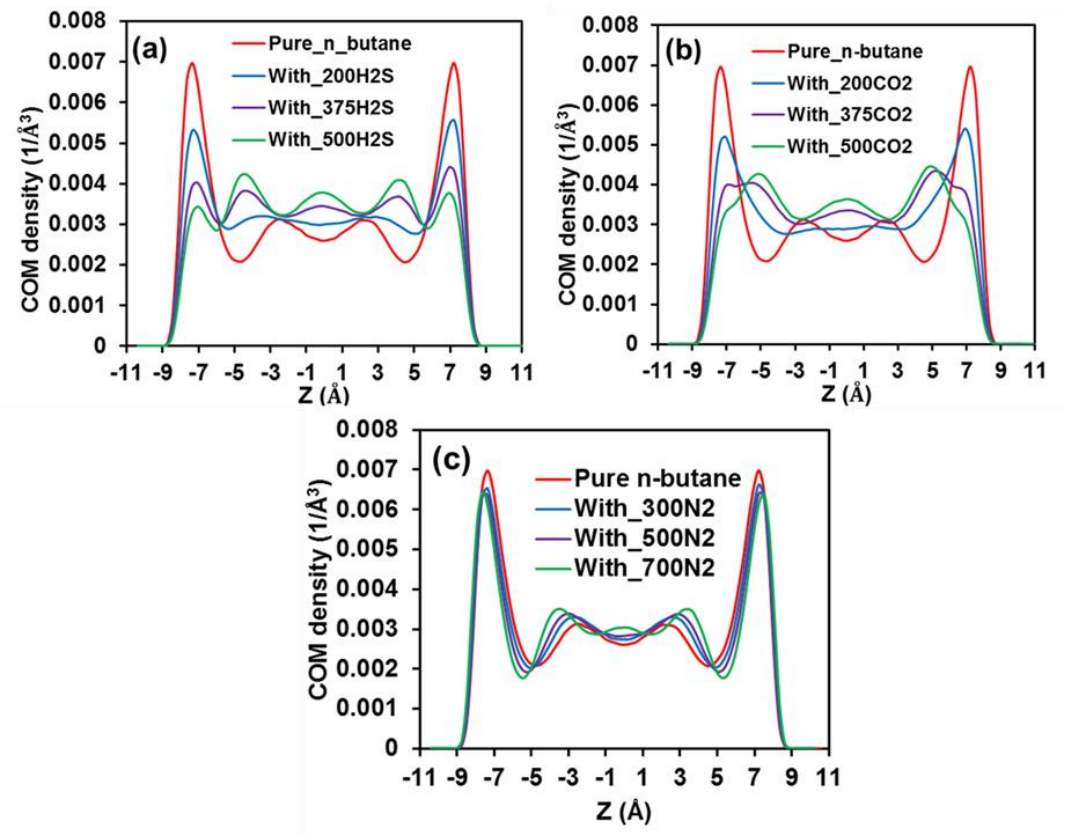

Figure 2: Density profile of the COM of *n*-butane in the binary system with H_2S loading (a), CO_2 loading (b) and N_2 loading (c). The density profile for a system with pure *n*-butane is also shown for comparison. All systems contain 300 *n*-butane molecules.

For completeness, we also simulated systems of *n*-butane in silica pores in the presence of N_2, without acid gases. The density profiles of COM of *n*-butane and N of N_2 for the binary systems are shown in **Figure 2c** and **3e**, respectively. The *n*-butane density profiles remain almost unchanged despite the presence of N_2. Comparing the density profiles of CO_2 and H_2S in **Figure 3** to that of N_2 in **Figure 3e** shows that the acid gases are more strongly adsorbed on the silica surface than N_2 as the peak heights within the FAL are higher. The density profile of N_2 in **Figure 3e** shows that more N_2 occupy the middle of the pore, where it probably mixes with *n*-butane and potentially reduces its viscosity. To test this latter possibility, we simulated bulk systems with densities approximately equal to those in the middle of the pore. We calculated the viscosity using the procedure described elsewhere,[56] and we obtained 0.16cP for pure *n*-butane and 0.21 and 0.24cP for *n*-butane-N_2 systems containing 200 n-butane and 200 N_2 molecules. These results suggest that N_2 increases the viscosity in the simulated pores, which is opposite of what was expected. This however is probably a consequence of the fact that the confined system becomes denser upon N_2 addition. Infact, the viscosity increases with pressure, as shown in **SI**.

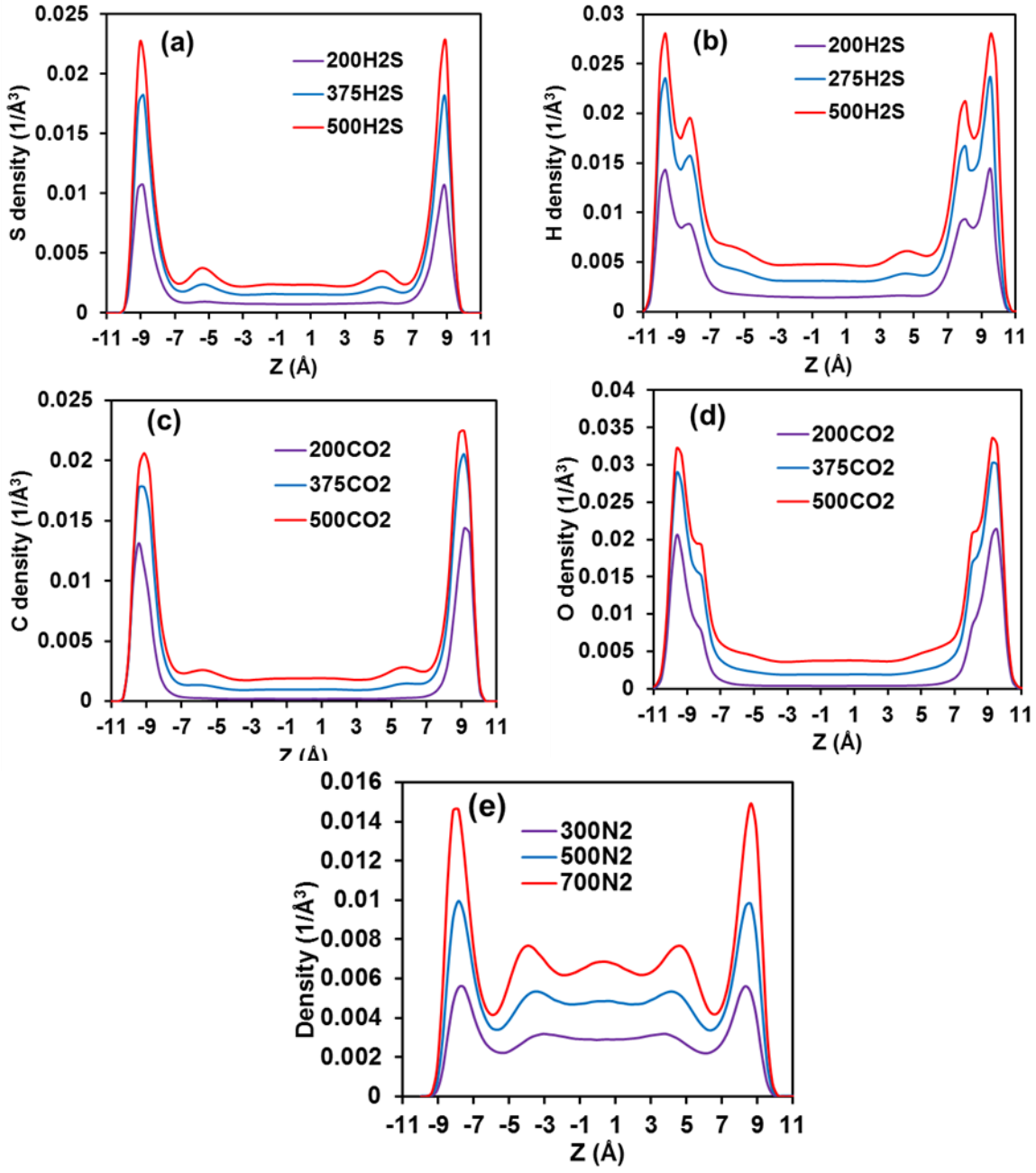

Figure 3: Density profile of S of H_2S (a) H of H_2S (b) C of CO_2 (c) O of CO_2 (d) and N of N_2 (e) in the binary systems at different acid gas and N_2 loadings in silica pores.

3.1.2 Interaction energy in silica pores

To quantify the fundamental mechanism responsible for the results summarised in **Table 3**, we calculated the interaction energy between selected fluid molecules and the silica substrate. For the *n*-butane-surface interaction energy, we calculated the corresponding LJ potential. The Coulombic potential is not considered as *n*-butane is not charged in our model. Plots of interaction energy versus

simulation time for all fluid molecules over the last 10ns of the simulations are presented in Figure S2 of the **SI** and show that the interaction energies of the systems are stable. The *n*-butane-surface interaction energy, normalized by the number of *n*-butane is shown in **Table 4**. The results are consistent with an attraction between *n*-butane and the pores. As H_2S or CO_2 are added to the system, the *n*-butane – pore interaction energy becomes less attractive. This result is qualitatively consistent with the percentage displaced of *n*-butane shown in **Table 3**, as higher percentage displaced correlates with less attractive interaction energy.

We also determined the CO_2-pore and H_2S-pore interaction energies ($E_{CO2\text{-}pore}$ and $E_{H2S\text{-}pore}$). For these calculations, we considered both LJ and electrostatic contributions to the interaction energy. The results are normalised by the amount of CO_2 or H_2S in the system. The results, presented in **Table 5** show that CO_2 is more strongly attracted to the pore surfaces than H_2S. This difference could explain why CO_2 is more effective than H_2S at reducing *n*-butane density near the silica pore surface. The results also indicate that the normalised interaction energy is more attractive when fewer acid gas molecules are present in the system. This is consistent with previous reports for CO_2-CH_4 confined in calcite[25] and in silica pores,[57] and suggests that the first acid gas molecules in the system adsorb on the preferential adsorption sites, possibly via electrostatic interactions related to the formation of hydrogen bonds. For the specific conditions considered, the preferential adsorption sites are expected to be the –OH groups on the surface. Analysis of our simulations suggests that 232 CO_2 and 238 H_2S molecules saturate each of the 2 pore surfaces available in our simulations. Density profiles in **Figure 3** show that some molecules of both CO_2 and H_2S occupy the region close to the centre of the pore even before the surface becomes saturated, suggesting some exchange between adsorbed and pore gases.

Table 4: *n*-Butane interaction energy with silica. All systems contain 300 *n*-butane molecules

Acid gas loading	With H_2S (kJ/mol)	With CO_2 (kJ/mol)
200	-3.13±0.01	-3.10±0.01
375	-2.65±0.02	-2.51±0.02
500	-2.37±0.02	-2.23±0.01
Pure *n*-butane	-3.74±0.01	

Table 5: Gas-silica pore interaction energy for H_2S and CO_2.

Gas Loading	$E_{H2S\text{-}Surf}$ (Electrostatic)(kJ/mol)	$E_{H2S\text{-}Surf}$ (LJ) (kJ/mol)	$E_{CO2\text{-}Surf}$ (Electrostatic)(kJ/mol)	$E_{CO2\text{-}Surf}$ (LJ)(kJ/mol)
200	-10.63±0.09	-2.77±0.01	-18.0±0.1	-4.05±0.02
375	-9.31±0.05	-2.57±0.01	-13.5±0.1	-3.35±0.01
500	-8.54±0.03	-2.42±0.01	-11.2±0.2	-2.94±0.01

3.1.3 Residence times

To further characterise the systems considered in **Figure 2**, we calculated the residence time via the residence correlation function (RCF), $C_R(t)$, for *n*-butane molecules found within a distance of 5Å from the pore surface, which belongs to the first adsorbed layer. The $C_R(t)$ is defined as:[37]

$$C_R = \frac{\langle N_i(t) N_i(0) \rangle}{\langle N_i(0) N_i(0) \rangle} \qquad (2)$$

In Eq. 2, $N_i(t) = 1$ if molecule i resides in the layer considered at time t, and 0 otherwise. $N_i(0) = 1$ if molecule i belongs to the layer at time $t = 0$ and becomes 0 only when molecule i leaves the layer and remains equal to zero even though the molecule returns to the layer. The faster $C_R(t)$ decays from 1 to 0, the faster molecules leave the layer considered, which in our case is the FAL. The COM of *n*-butane is used to represent the position of one *n*-butane molecule in this calculation. The $C_R(t)$ calculated for *n*-butane as a function of H_2S and CO_2 loading are shown in **Figure 4**. The results show that in both *n*-butane-H_2S and *n*-butane-CO_2 systems, the autocorrelation functions decay to zero faster as the gas loading increases. Comparing results obtained for H_2S with CO_2 at the same loading shows faster decays in the presence of CO_2. This suggests that the interactions between CO_2 and the pore surface weaken the surface-*n*-butane interactions more effectively than those between H_2S and the surface. The $C_R(t)$ for H_2S and CO_2 molecules in the first adsorbed layer are shown in **Figures 4c** and **4d**. We considered the C of CO_2 and the S of H_2S for the $C_R(t)$ calculation. The results show that the residence times of gas molecules in the first adsorbed layer decreases as loading increases. This is probably due to fast exchange between gas molecules in the adsorbed layer and those close to the centre of the pore. This observation is consistent with previous reports in literature,[24] with our density profiles, and also with the interaction energies discussed above.

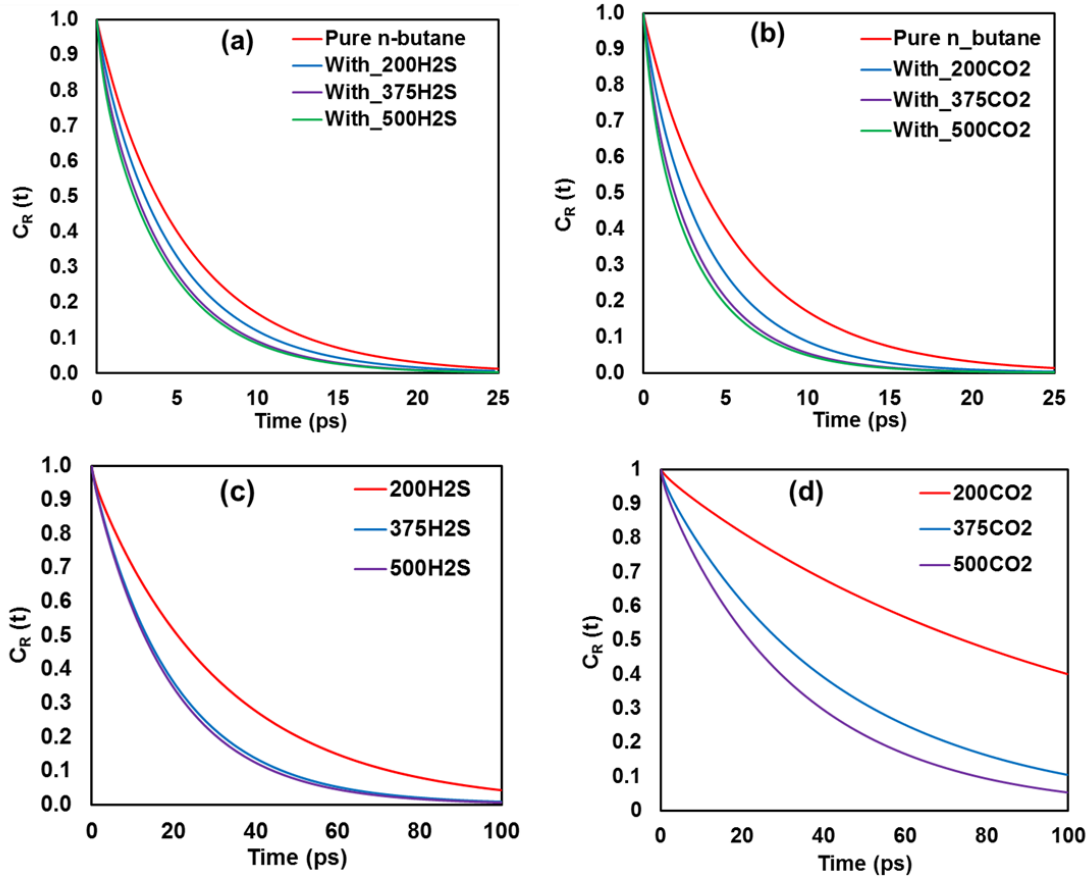

Figure 4: Residence CF for *n*-butane molecules in the FAL at different H_2S (a) and CO_2 loading (b). The CF for system containing pure *n*-butane is also shown for comparison. CF of H_2S molecules in the FAL at different loading are shown in (c) and for CO_2 molecules at different loading in (d).

3.2 Ternary Systems

3.2.1 Effect of H_2S-CO_2 mixtures on n-butane displacement

To investigate whether mixtures of H_2S and CO_2 could act synergetically in terms of *n*-butane displacement from the pore surfaces, we quantified the effect of 50%-50% mixtures of CO_2 and H_2S in the presence of *n*-butane (system 10 in **Table 1**). The corresponding *n*-butane density profiles are compared in **Figure 5a**. The results show that the distribution of *n*-butane in the presence of the H_2S - CO_2 mixture is between those obtained when either CO_2 or H_2S is present, yielding a percentage displaced of ~ 62%. These results suggest that mixing these gases is not synergetic, but rather reduces the ability of CO_2 to displace *n*-butane from the pore surfaces by ~5%. This is consistent with the report of Khan et al.,[34] who used reservoir simulations to quantify the effect of acid gas injection on

enhanced gas recovery. Results for the *n*-butane $C_R(t)$, shown in **Figure 5b**, are also consistent with what has just been discussed.

To further understand how H_2S-CO_2 mixtures could displace *n*-butane from pore surfaces, we simulated additional ternary systems varying the gas composition while maintaining a constant acid gas loading of 375 molecules. We simulated CO_2:H_2S ratios of 1:2 and 2:1 (systems 11 and 12 in **Table 1**). The density profiles, presented in **SI**, suggest that the higher the CO_2 fraction in the gas mixture, the better the displacing performance.

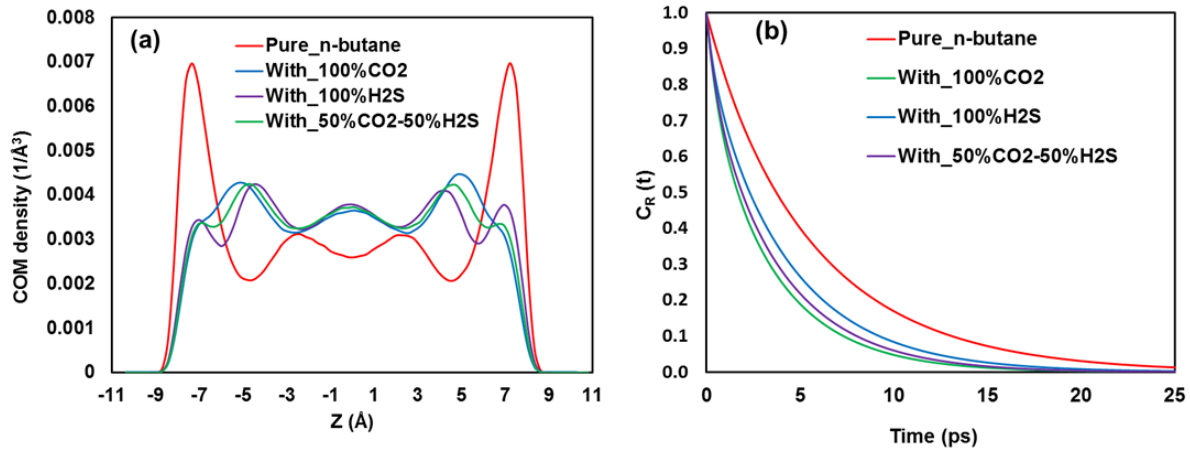

Figure 5: Comparison of density profiles of n-butane in the presence of pure CO_2 and H_2S and their mixture (a) and residence CF for the same systems (b). The binary systems contain 300 n-butane and 500 molecules of the gases. The mixture comprises 250 molecules for each of the acid gas.

3.2.2 Effect of CO_2/H_2S/N_2 mixture composition on *n*-butane displacement

The results discussed so far suggest that the ability of H_2S and CO_2 to displace hydrocarbons from the pore surface is related to their strong pore-wall attractions, sometimes due to electrostatic interactions. To further test this observation, we conducted additional simulations in which nitrogen was added to various systems. We conducted simulations for 80%CO_2-20%N_2 and 60%CO_2-40%N_2 for a total gas loading of 500 molecules (systems 15 and 16 in **Table 1**), as well as for systems containing H_2S and N_2 (systems 13 and 14 in **Table 1**). The results are shown in **Figure 6**. The density profiles for COM of *n*-butane are shown in **Figure 6a** and **6b** and those for C of CO_2, S of H_2S and N of N_2 in **Figure 6c** and **6d**. The estimated percentage displaced for the various systems is shown in **Figure 6e** and **6f**. The results show that as the N_2 mole fraction in the mixture increases, the percentage displaced decreases.

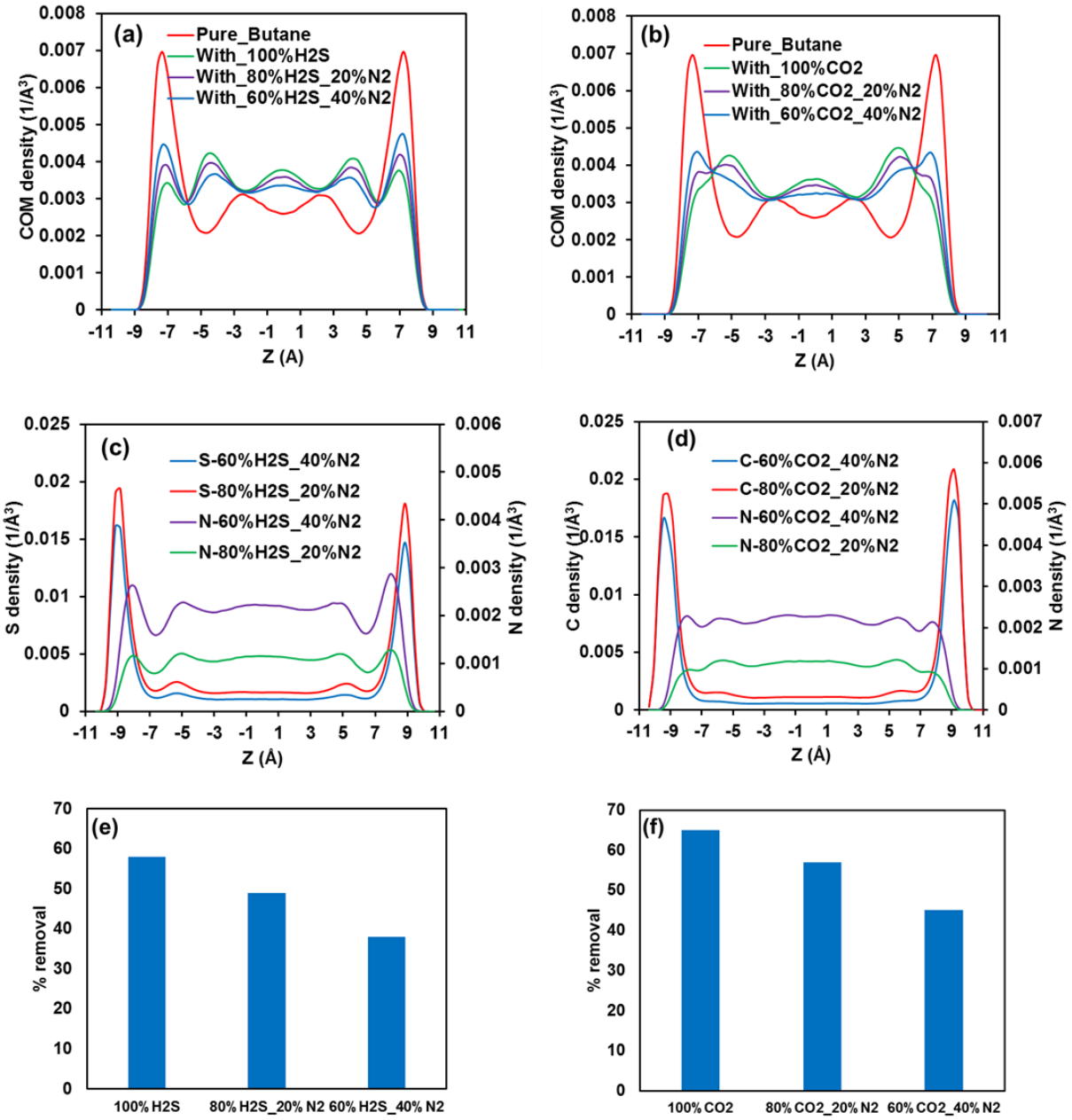

Figure 6: Density profiles for COM of *n*-butane for (a) H_2S-N_2 system (b) CO_2-N_2 system. Density profiles for N of N_2 for (c) H_2S-N_2 (d) CO_2-N_2 systems. There are 300 *n*-butane molecules in all cases. The total number of gas molecules is 500. Percentage of hydrocarbon displaced is also shown for H_2S-N_2 (e) and CO_2-N_2 systems (f).

3.3 Effect of Pore Surface Chemistry

3.3.1 Density profiles and percentage displaced

To investigate whether the performance of the acid gases depends on the nature of the substrate, we performed additional simulations in muscovite and magnesium oxide (MgO) pores. The corresponding system compositions are shown in **Table 1.** The CO_2 and H_2S gases were added into pores containing 300 *n*-butane molecules. The number of *n*-butane molecules is constant for all systems. It should be noted that the bulk pressures corresponding to systems with H_2S and CO_2 are similar (see **Table 2**). The density profiles for the COM of *n*-butane at different loadings are shown in **Figure 7**. The calculated percentage *n*-butane displaced from the pore surfaces are presented in **Figure 8**. The results show (a) higher percentage displaced for H_2S than CO_2 in muscovite; (b) both gases yield similar, rather poor performance in MgO. It should be noted that the pressures considered in the silica substrate (see **Table 2**) are somewhat different compared to those considered in the other two substrates. However, because the results are due to preferential fluid-surface interactions, we do not expect this difference to affect qualitatively the results presented. These results are certainly dependent on the protonation states of the surfaces considered here, as these affect the interactions between the various fluid molecules and the pore surfaces. Because water was not considered in our systems, we did not explicitly quantify the effect of varying surface protonation on the results presented. The density profiles of carbon and oxygen of CO_2, sulphur and hydrogens of H_2S and N of N_2 for binary systems in silica and MgO pores are shown in **SI**. In all cases, CO_2 and H_2S are preferentially adsorbed on the surfaces.

Results for *n*-butane-pore interaction energies (**Figure 9)** show that both CO_2 and H_2S reduce *n*-butane – pore attraction except in MgO, in which case the interaction energy remains relatively unchanged upon gas loading. The results for the normalised interaction energies between the gases and the substrates, shown in **Figure 10**, show that, while CO_2 is more strongly attracted to silica than H_2S, H_2S is more strongly attracted to muscovite than CO_2. Both gases have similar interaction with MgO. These results suggest that the more strongly a gas is attracted to a porous substrate, the more effective it is expected to be at diplacing hydrocarbons from the surface of the corresponding pore.

Results for *n*-butane residence correlation function, $C_R(t)$ are described in **SI**, and indicate that: (a) in silica, the residence time of *n*-butane decreases with H_2S and CO_2 loadings; (b) in muscovite, $C_R(t)$

essentially overlap as CO_2 loading changes, suggesting that *n*-butane exchange between adsorbed molecules close to the pore walls and to the pore centre occurs with similar frequency irrespective of CO_2 loading; (c) for H_2S loading in muscovite, residence time decreases with loading; and (d) in MgO pores, $C_R(t)$ increases with increase in H_2S and CO_2 loading.

In general, the results just discussed suggest that, for dry systems, it is possible to identify those gases that can more effectively displace short linear hydrocarbons from the pore surfaces by considering the interactions of such gases with the solid themselves: the gases that are more strongly attracted to the pore surfaces are likely to be more effective at displacing the hydrocarbons. Because realistic materials are heterogeneous, lab-scale experimental tests should be conducted before field campaigns.

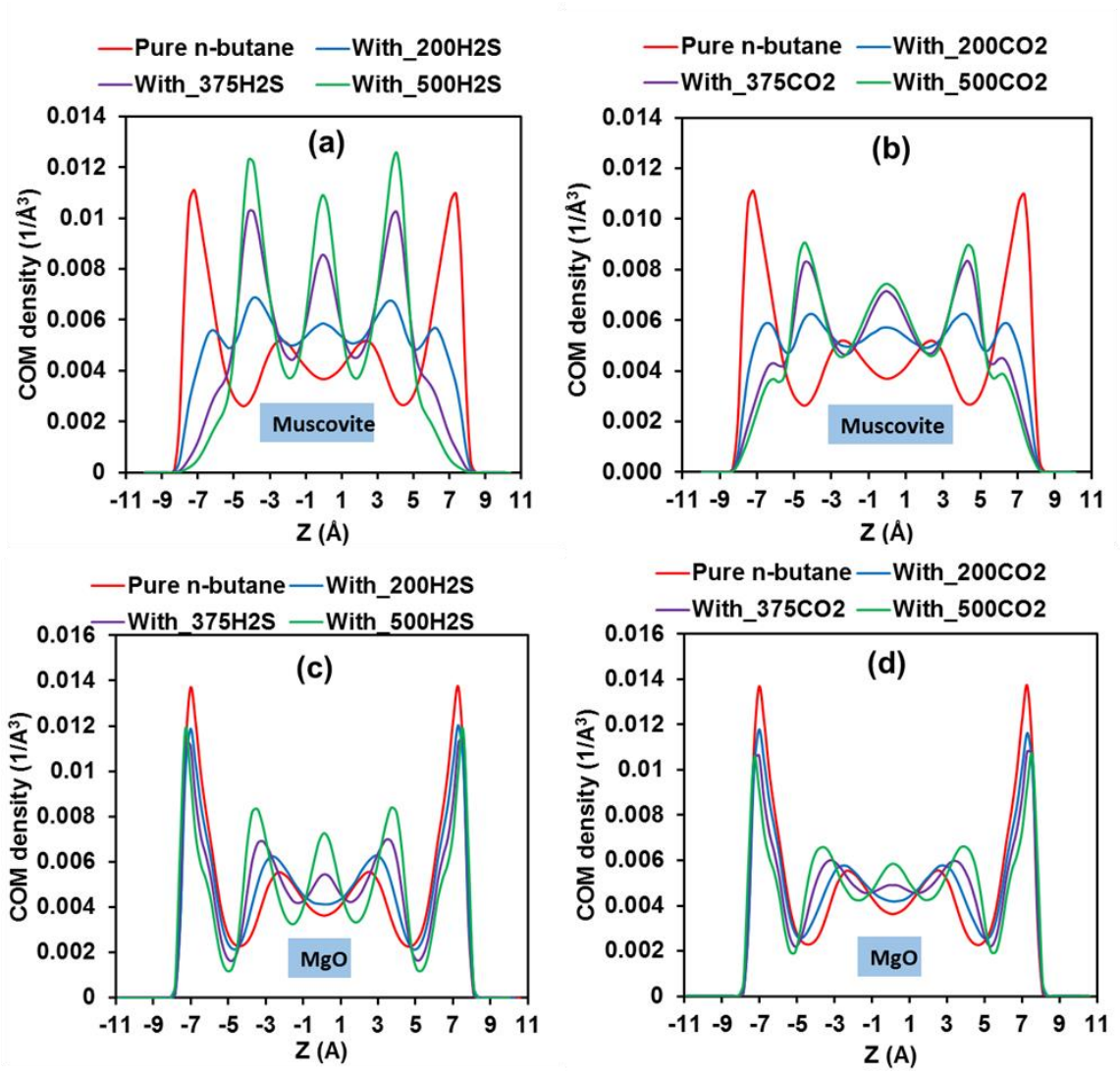

Figure 7: *n*-Butane density profiles at different gas loadings for H_2S in muscovite (a) CO_2 in muscovite (b) H_2S in MgO (c) and CO_2 in MgO (d). The system comprises 300 *n*-butane molecules in all cases.

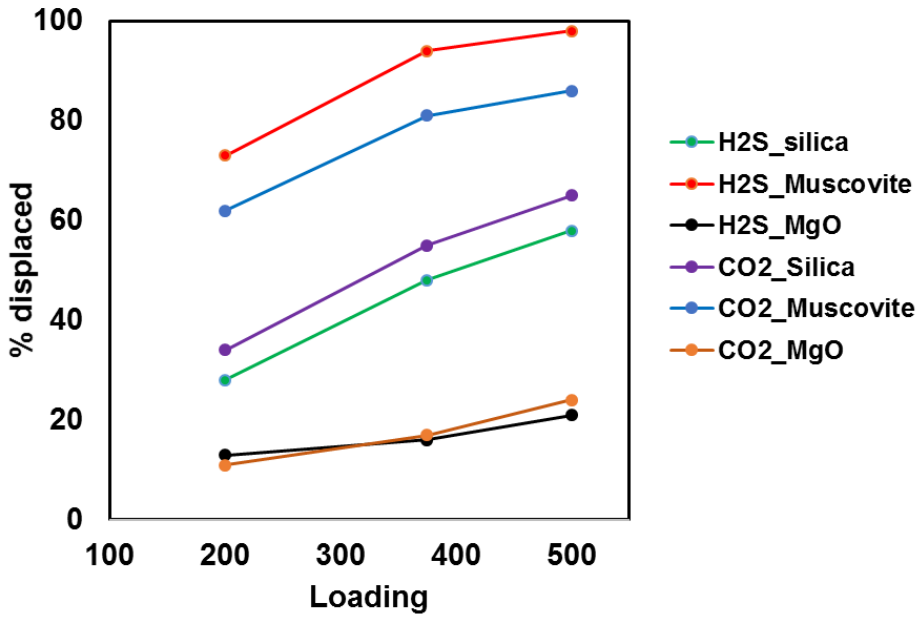

Figure 8: Percentage of *n*-butane displaced by H_2S and by CO_2 in the substrates considered.

3.3.3 Effect of nitrogen in muscovite and MgO pores

Additional simulations were conducted in which nitrogen was added to the confined systems instead of the other gases. The results, shown in **SI**, are consistent with those discussed for silica pores and suggest that N_2 has little or no effect on *n*-butane displacemement from the pore surfaces even when muscovite or MgO pores are considered. In all cases, nitrogen seems to preferentially distribute near the pore centre.

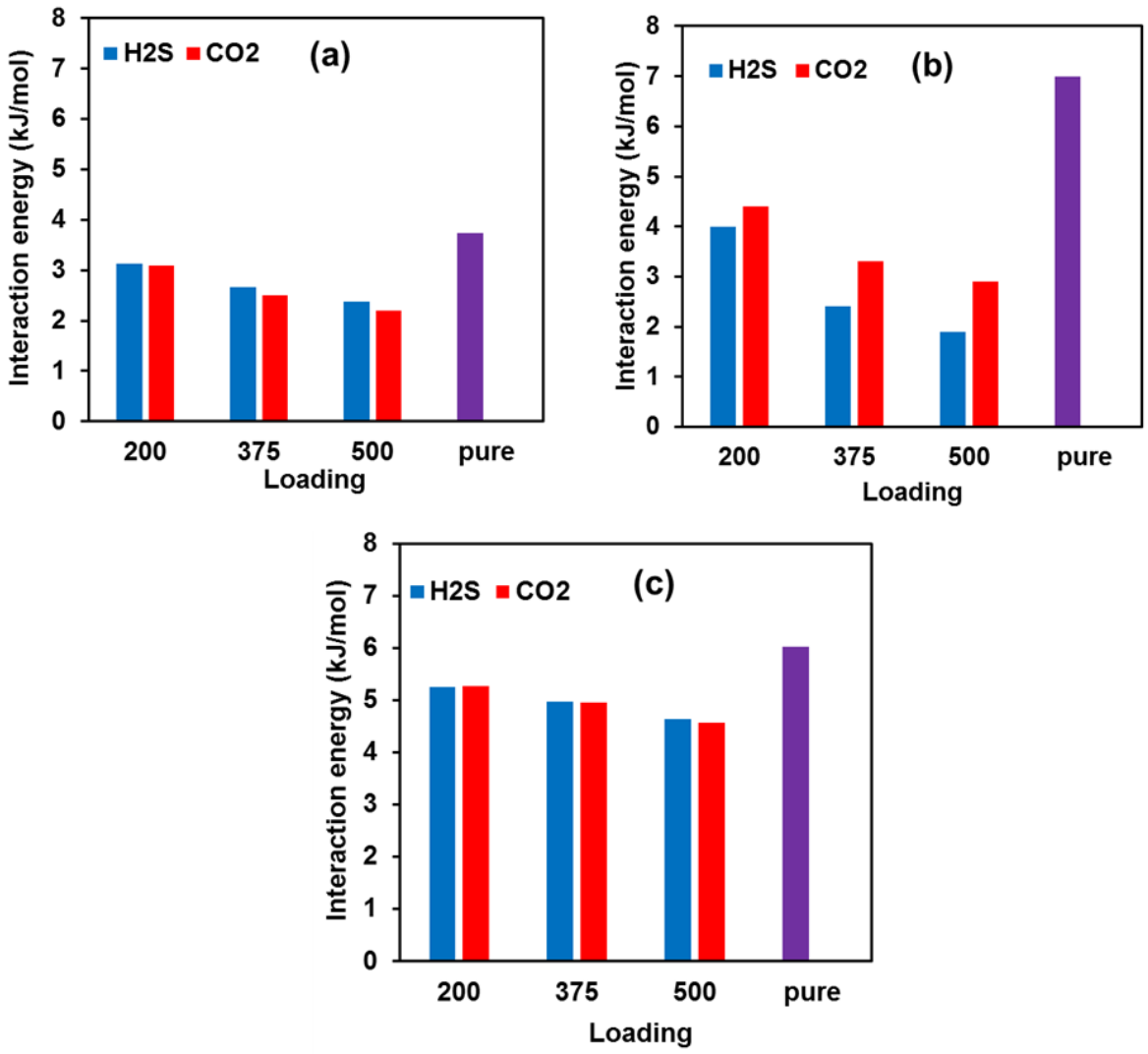

Figure 9: Magnitude of total interaction energy of *n*-butane at different gas loading for silica (a) muscovite (b) and MgO (c). The systems comprise 300 *n*-butane molecules and various amounts of the other fluids. The interaction energies are normalised by the number of *n*-butane molecules in the system. The interaction energy shown is only due to van der Waals interaction as *n*-butane molecules bear no charge.

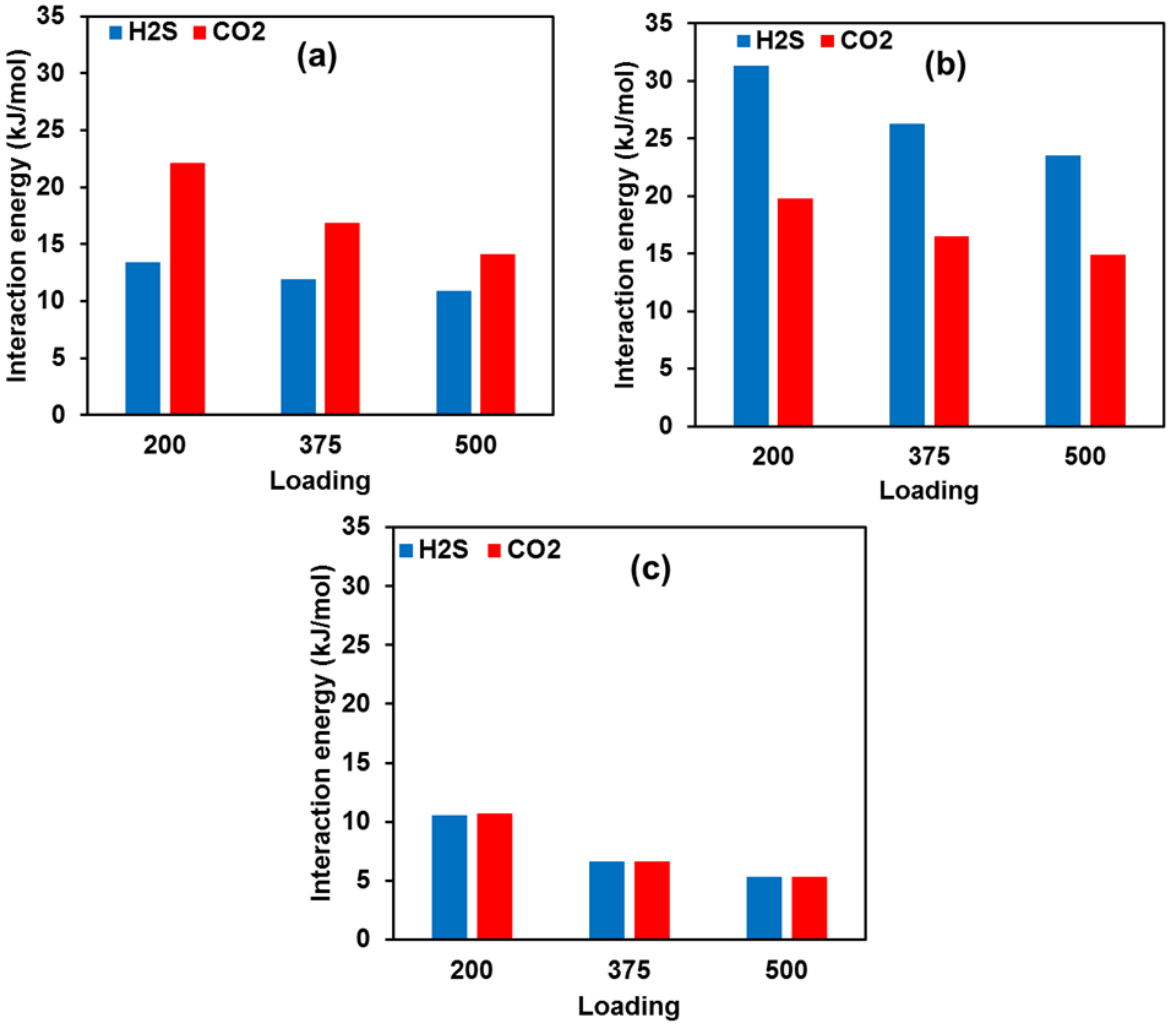

Figure 10: Magnitude of total interaction energy of CO_2 and H_2S at different loading for silica (a) muscovite (b) and MgO (c). The systems comprise 300 *n*-butane molecules in all cases. The interaction energies are normalised by the number of gas molecules in the system. The interaction energy shown is the sum of the LJ and electrostatic contributions.

3.4 Molecular Structure of Adsorbed Gases

The results above demonstrate that different gases can have various effects in displacing short linear hydrocarbons from pore surfaces because of their different interactions with the pore surfaces. Because the interaction energies depend on the various chemical species found on the pore surface, it is of fundamental interest to quantify how the various fluid molecules assemble within a pore, with relevance to the distribution of the atomic species on the solid substrate. We consider here gas molecules adsorbed within the FAL, because of the relevance of the FAL, based on our prior results, on determining the distribution and the diffusion coefficients of various fluid molecules within narrow pores.[24]

3.4.1 Orientation of adsorbed gases in the first adsorbed layer

We provide the preferential orientation of CO_2 and H_2S molecules in contact with all simulated substrates in **Figure 11a** and **11b**, respectively. The molecules considered in the calculation are those found within 2Å from silica and muscovite surfaces and 5 Å from MgO surface. The results are obtained at the maximum loading conditions. The thickness of the adsorbed layers considered (i.e., 2 vs. 5 Å), is chosen based on the features of the density profiles, to focus on the FAL. The orientation of CO_2 molecules were quantified in terms of the distribution of the angle formed between the CO_2 backbone and the surface normal. If the angle equals 0° or 180°, CO_2 is perpendicular to the surface, when it is 90°, CO_2 lays parallel to the surface. For H_2S, we plot the distribution of the angle formed between the vector pointing from S to the midpoint of H-H vector and the surface normal. When the angle equals 0°, H_2S points the two hydrogen atoms away from the surface, and when it is 180°, H_2S points both hydrogens towards the surface. When theta is 90°, H_2S either points one hydrogen to the surface or lays parallel to the surface. **Figure 11a** and **11b** show that the gases adopt different orientation on each of the substrates. On silica, CO_2 yields an angle of ~ 75° to the surface. A similar orientation of CO_2 has been previously reported for silica.[23] For muscovite and MgO, in the models considered here, CO_2 lays parallel to the surface. On the other hand, H_2S on muscovite is almost in 2-hydrogen down orientation, while on silica and MgO its orientation seems to be with either one hydrogen towards the surface or parallel to it. The results show that the nature of the substrates dictates the structure of adsorbed gas, which could influence the EOR performance of the gas. For example, H_2S tends to perform better than CO_2 in muscovite where it almost points its two hydrogen atoms towards the surface when compared to its performance in silica where it preferentially points one hydrogen down or lays parallel to the surface. Note that CO_2 performs better than H_2S in silica. This suggests that H_2S could be effective at displacing hydrocarbons from substrates in which active sites are available on the solid surfaces where both hydrogen atoms of H_2S could be strongly attracted.

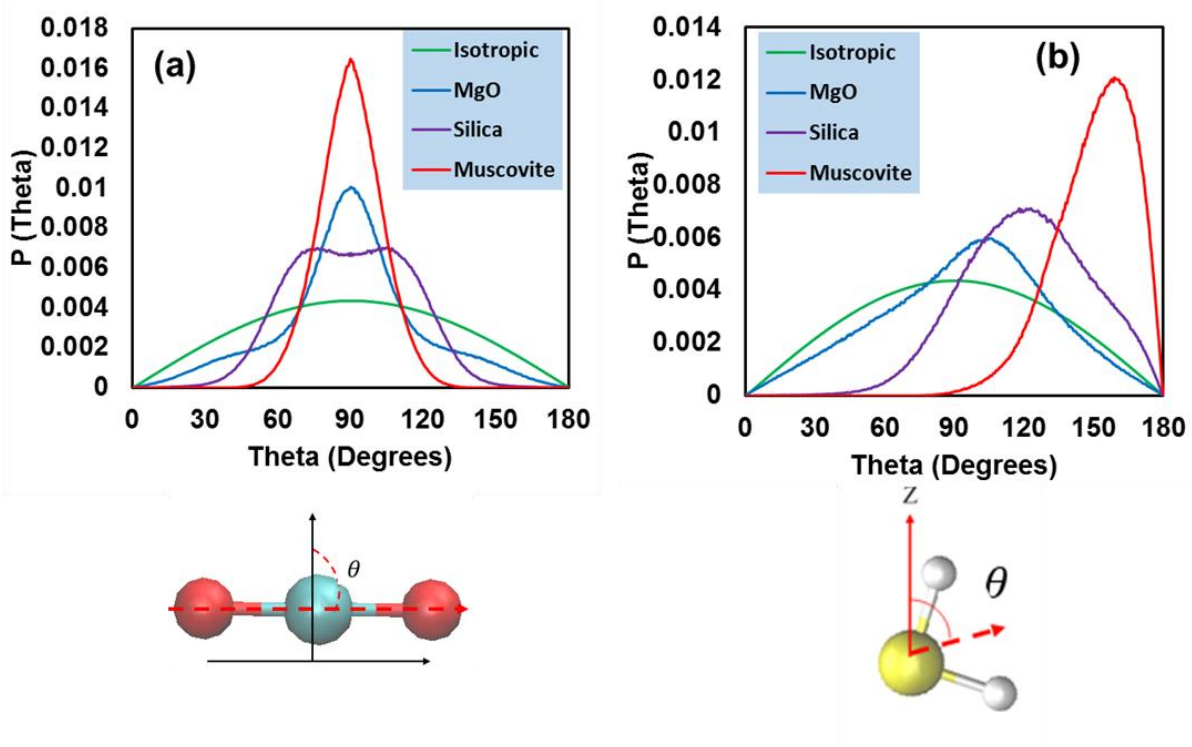

Figure 11: (a) Probability distribution of angle theta for CO_2 molecules (a) and H_2S molecules (b) adsorbed within 2Å from silica and muscovite surfaces and 5Å from MgO surface. The results are compared with the isotropic distribution (green). All systems contain 300 *n*-butane and 500 acid gas molecules.

3.4.2 Planar density distributions

To further quantify how the solid substrates determine the distribution of H_2S within the FAL, we study the in-plane density distributions of H_2S and we relate it to the atomic distribution on the three surfaces. In **Figure 12**, we present the in-plane density distribution of sulphur (S) of H_2S in all simulated substrates. The correspondent results for the hydrogen atoms (H) of H_2S are shown in **SI**. The results reveal the preferential adsorption sites for H_2S. For example, on silica, S of H_2S preferentially interacts with the vertices of the hexagonal rings formed by the silicon atoms of the substrate. In muscovite, S of H_2S preferentially adsorbs on the hydroxyl groups in muscovite interlayer. On the other hand, for MgO, S of H_2S adsorbs near the oxygen atoms.

Similar results are shown in **SI** for CO_2.

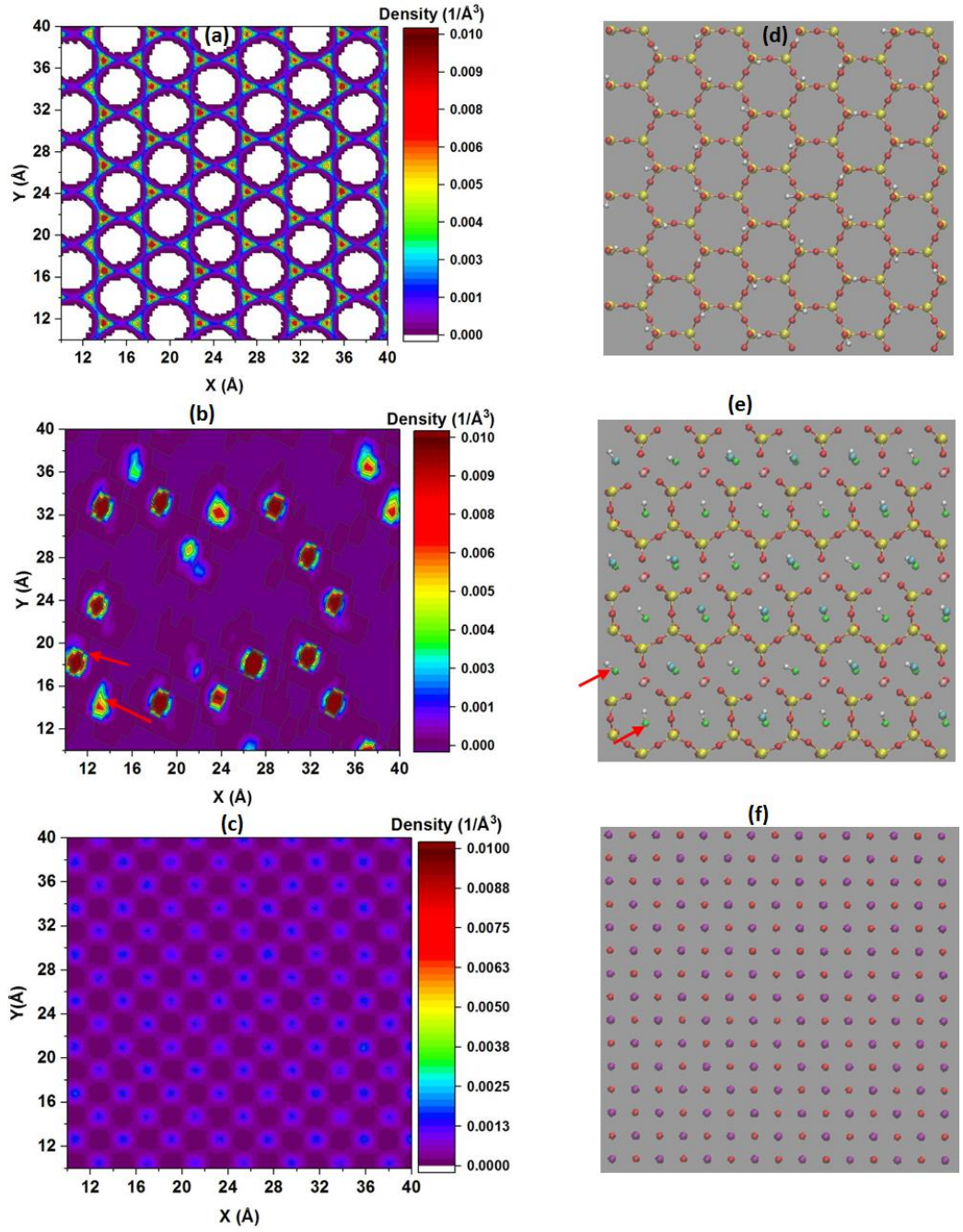

Figure 12: In-plane density distribution of S of H_2S at contact with (a) silica (b) muscovite (c) MgO. Snapshot of silica (d) muscovite (e) and MgO (f) are also shown. All systems contains 500 H_2S and 300 *n*-butane. Colour code: OH oxygen - green , bridging oxygen – red, silicon – yellow, potassium – cyan, purple – magnesium, hydrogen – white.

3.5 Diffusion Coefficients of Confined Fluids

To quantify the diffusion coefficients, we followed established procedures, starting from the mean square displacement (MSD) of the COM of *n*-butane, acid gases, and N_2 as a function of time (shown in Supporting Information).[58] The diffusion coefficient results presented in **Tables 6-8** show that CO_2,

H_2S and N_2, in general, slow down the diffusion of *n*-butane in all simulated substrates, probably because of pore crowding. An exception is in the case of the lowest CO_2 loading (200 CO_2) in silica, wherein the self diffusion coefficient obtained for *n*-butane is slightly higher than that observed for the pure *n*-butane when no CO_2 is present. To check whether CO_2 could enhance the *n*-butane diffusion at lower loading ("molecular lubrication"), we simulated additional systems where 300 *n*-butane molecules were simulated together with either 125 or and 75 CO_2 molecules. We obtained 6.4 x 10^{-8} and 6.5 x 10^{-8} m^2/s for *n*-butane diffusion coefficient when 75 and 125 CO_2 molecules were present within the silica pore, respectively. These results are similar to those obtained for pure *n*-butane, suggesting that CO_2 could enhance *n*-butane transport, but that pore crowding quickly suppresses this effect, at the conditions considered in this report. For completeness, the self-diffusion coefficients obtained for CO_2 when either 75 or 125 CO_2 molecules were present together with 300 molecules of *n*-butane were found to be 2.7 x 10^{-9} and 3.9 x 10^{-9} m^2/s, respectively.

Table 6: Self-diffusion coefficient for *n*-butane, CO_2, H_2S, and N_2 in silica pores. Please refer to **Table 1** for system composition.

System	D(*n*-butane) (10^{-8} m^2/s)	D(H_2S) (10^{-8} m^2/s)	D(CO_2) (10^{-8} m^2/s)	D(N_2) (10^{-8} m^2/s)
1	6.5±0.1	1.8±0.02	-	-
2	6.2±0.2	1.5±0.02	-	-
3	5.5±0.2	1.3±0.04	-	-
4	7.0±0.4	-	0.6±0.03	-
5	6.4±0.3	-	1.0±0.01	-
6	6.6±0.4	-	1.1±0.01	-
7	5.8±0.2	-	-	4.2±0.05
8	5.8±0.2	-	-	2.6±0.04
9	5.2±0.1	-	-	2.0±0.04
Pure n-butane	6.5±0.2	-	-	-

The results in **Tables 6-8** show that H_2S and CO_2 have lower self-diffusion coefficients than *n*-butane, reflecting the stronger interaction with the substrates, as discussed above. The results suggest that H_2S travels faster than CO_2 through the silica pores, consistent with the weaker attraction to this substrate. In muscovite pores, CO_2 travels faster than H_2S while both acid gases has similar diffusion coefficient in MgO pores. These results are consistent with interaction energy results presented in **Figure 10**. Results in **Tables 6-8** also show that N_2 travels faster than H_2S and CO_2 especially at low N_2 loading, perhaps due to smaller size of N_2 molecule and also reflecting the fact that N_2 does not show strong adsorption to the pore surfaces in the systems considered here.

Some prior studies reported an enhancement of the mobility of hydrocarbons within model pores upon low CO_2 loading.[24, 26, 59] This was not observed in the present simulations, because the systems

considered here are very dense, and pore crowding is expected to inhibit diffusion. In fact, prior studies have reported a decrease in hydrocarbon mobility at higher CO_2 loadings.[59]

Table 7: Diffusion coefficients for *n*-butane, CO_2, H_2S, and N_2 in muscovite pores. Please refer to **Table 1** for system composition.

System	D(*n*-butane) (10^{-8} m^2/s)	D(H_2S) (10^{-9} m^2/s)	D(CO_2) (10^{-9} m^2/s)	D(N_2) (10^{-9} m^2/s)
1	3.7±0.1	3.7±0.1	-	-
2	3.5±0.3	3.1±0.1	-	-
3	2.9±0.2	1.9±0.1	-	-
4	3.8±0.3	-	4.8±0.1	-
5	3.5±0.2	-	3.4±0.1	-
6	2.9±0.1	-	2.5±0.1	-
7	0.9±0.2	-	-	5.3±0.3
8	0.9±0.1	-	-	2.6±0.2
9	0.7±0.1	-	-	1.0±0.2
Pure *n*-butane	4.1±0.2	-	-	-

Table 8: Diffusion coefficients for *n*-butane, CO_2, H_2S, and N_2 in MgO pores. Please refer to **Table 1** for system composition.

System	D(*n*-butane) (10^{-8} m^2/s)	D(H_2S) (10^{-9} m^2/s)	D(CO_2) (10^{-9} m^2/s)	D(N_2) (10^{-9} m^2/s)
1	3.1±0.2	11.4±0.2	-	-
2	2.3±0.1	5.9±0.1	-	-
3	2.0±0.2	3.7±0.1	-	-
4	3.4±0.3	-	11.3±0.1	-
5	2.7±0.1	-	5.9±0.1	-
6	2.3±0.2	-	3.7±0.1	-
7	3.3±0.2	-	-	16.5±0.4
8	2.1±0.2	-	-	8.1±0.3
9	2.4±0.1	-	-	3.1±0.2
Pure *n*-butane	4.2±0.3	-	-	-

4 CONCLUSIONS

Equilibrium MD simulations were performed to investigate the energetics, structure and transport properties of *n*-butane confined within slit-shaped nano-pores of width 2.2 nm carved out of silica, muscovite and MgO surfaces, in the presence of various amounts of CO_2, H_2S, N_2 and their mixtures at 350K. The study compares the effect of H_2S vs. that of CO_2, the effect of the presence of an inert gas (N_2), and the effect of pore-surface chemistry on the behaviour of confined hydrocarbons. Because all

the pores considered were dry, pH effects on the pore surfaces were not investigated. Our results show that CO_2 is more efficient than H_2S in displacing *n*-butane from silica surfaces, while H_2S is more effective than CO_2 in muscovite. The two gases show similar performance in MgO. Analysis of the fluid-substrate interaction energy reveals that these results strongly correlate with the attraction between each acid gas and the pore surface. While H_2S is more strongly attracted to muscovite compared to CO_2, it is more weakly adsorbed on silica. Both gases show similar interaction with MgO. Our results also show that mixtures of CO_2 and H_2S do not yield synergetic effects in displacing *n*-butane. The orientation and planar distribution of the adsorbed acid gases on the three solid surfaces further reinforce the observation that the nature of the pore surface dictates the structure of the adsorbed fluids, thus affecting how the acid gases control the structure of confined hydrocarbons. In most cases considered, our results show that the self-diffusion coefficient of *n*-butane decreases when other gases are added. This is probably due to a pore-crowding effect. Our results could contribute to the design of enhanced oil recovery strategies for improvement in hydrocarbon production and in acid gas sequestration. Future investigations should address the effect of water on the results presented.

SUPPORTING INFORMATION

The Supporting Information is available free of charge on the ACS Publications website at DOI:

System composition determination; pressure calculation procedure; viscosity of bulk n-butane – N_2 systems; interaction energy as a function of time; simulation snapshots for n-butane – CO_2 and n-butane – N_2 systems; density profiles of n-butane –CH_3, -CH_2 and COM in silica pores; density profiles of n-butane for gas mixtures at different ratios; density profiles of S of H_2S, H of H_2S, C of CO_2, O of CO_2 and N of N_2 for binary systems of *n*-butane-acid gas and *n*-butane-N_2 in muscovite and MgO pores; density profiles of the centre of mass of *n*-butane, S of H_2S, C of CO_2 and N of N_2 at different acid gas-N_2 ratios in the muscovite pores and MgO pores; we show the density profiles of *n*-butane for *n*-butane-N_2 systems in muscovite and MgO pores at different N_2 loadings. C_R (t) for the COM of *n*-butane for binary systems of *n*-butane-acid gas in muscovite and MgO pores; in-plane density distributions for H of H_2S within the FAL in silica, muscovite and MgO; in-plane density distribution of C and O of CO_2

in contact with the surface for all simulated pores; mean sqyare displacements for binary systems of *n*-butane – H_2S, n-butane – CO_2 and n-butane – N_2 in silica, muscovite and MgO pores.

ACKNOWLEDGEMENTS

Generous allocations of computing time were provided by the National Energy Research Scientific Computing Center (NERSC) at Lawrence Berkeley National Laboratory. NERSC is supported by the DOE Office of Science. S.B.B. acknowledges financial support from the Petroleum Technology Development Fund (PTDF). This research received funding from the European Union's Horizon 2020 research and innovation program under Grant No. 764810, within the consortium 'Science4CleanEnergy'. D.R.C. was supported by the U. S. Department of Energy, Office of Basic Energy Sciences, Division of Chemical Sciences, Geosciences and Biosciences under grant DE-SC0006878. We are grateful to Adrian Gregory and Prof. John Shaw for insightful discussions. Prof. Shaw's sabbatical at University College London was in part supported by the Leverhulme Trust under grant agreement number VP2-2017-023.

REFERENCES

1. Malik, Q. M.; Islam, M. In *CO_2 Injection in the Weyburn Field of Canada: Optimization of Enhanced Oil Recovery and Greenhouse Gas Storage with Horizontal Wells*, SPE/DOE improved oil recovery symposium, Society of Petroleum Engineers: **2000**.
2. Ghaderi, S. M. Simulation Study of CO_2 Injection and Storage in Alberta. PhD Thesis, University of Calgary, **2013**.
3. Benson, S. M.; Deutch, J. Advancing Enhanced Oil Recovery as a Sequestration Asset. *Joule* **2018**, *2*, 1386-1389.
4. Niemi, A.; Bensabat, J.; Shtivelman, V.; Edlmann, K.; Gouze, P.; Luquot, L.; Hingerl, F.; Benson, S. M.; Pezard, P. A.; Rasmusson, K. Heletz Experimental Site Overview, Characterization and Data Analysis for CO_2 Injection and Geological Storage. *Int. J. GreenH Gas Con.* **2016**, *48*, 3-23.
5. Clark, D. E.; Gunnarsson, I.; Aradottir, E.; Oelkers, E. H.; Sigfússon, B.; Snæbjörnsdottír, S.; Matter, J. M.; Stute, M.; Júlíusson, B. M.; Gíslason, S. R. In *Mineral Storage of CO_2/H_2S Gas Mixture Injection in Basaltic Rocks*, AGU Fall Meeting Abstracts, 2017.
6. Orr, F. M.; Heller, J. P.; Taber, J. J. Carbon Dioxide Flooding for Enhanced Oil Recovery: Promise and Problems. *J. Am. Oil Chem.' Soc.* **1982**, *59*, 810A-817A.
7. Fang, T.; Wang, M.; Gao, Y.; Zhang, Y.; Yan, Y.; Zhang, J. Enhanced Oil Recovery with CO_2/N_2 Slug in Low Permeability Reservoir: Molecular Dynamics Simulation. *Chem. Eng. Sci.* **2018**.
8. Yan, Y.; Dong, Z.; Zhang, Y.; Wang, P.; Fang, T.; Zhang, J. Co 2 Activating Hydrocarbon Transport across Nanopore Throat: Insights from Molecular Dynamics Simulation. *Phys. Chem. Chem. Phys.* **2017**, *19*, 30439-30444.
9. Gunnarsson, I.; Aradóttir, E. S.; Oelkers, E. H.; Clark, D. E.; Arnarson, M. Þ.; Sigfússon, B.; Snæbjörnsdóttir, S. Ó.; Matter, J. M.; Stute, M.; Júlíusson, B. M. The Rapid and Cost-Effective Capture and Subsurface Mineral Storage of Carbon and Sulfur at the Carbfix2 Site. *Int. J. GreenH Gas Con.* **2018**, *79*, 117-126.
10. Cole, D. R.; Striolo, A. The Influence of Nanoporosity on the Behavior of Carbon-Bearing Fluids. Whole Earth Carbon book chapter Carbon Reactivity: 2019.
11. Yuan, S.; Wang, S.; Wang, X.; Guo, M.; Wang, Y.; Wang, D. Molecular Dynamics Simulation of Oil Detachment from Calcite Surface in Aqueous Surfactant Solution. *Comput. Theor. Chem* **2016**, *1092*, 82-89.
12. Jessen, K.; Tang, G.-Q.; Kovscek, A. R. Laboratory and Simulation Investigation of Enhanced Coalbed Methane Recovery by Gas Injection. *Transport Porous Med.* **2008**, *73*, 141-159.
13. Kowalczyk, P.; Gauden, P. A.; Terzyk, A. P.; Furmaniak, S.; Harris, P. J. Displacement of Methane by Coadsorbed Carbon Dioxide Is Facilitated in Narrow Carbon Nanopores. *J. Phys. Chem. C* **2012**, *116*, 13640-13649.
14. Yan, Y.; Li, C.; Dong, Z.; Fang, T.; Sun, B.; Zhang, J. Enhanced Oil Recovery Mechanism of CO_2 Water-Alternating-Gas Injection in Silica Nanochannel. *Fuel* **2017**, *190*, 253-259.
15. Sheng, J. J.; Chen, K. Evaluation of the Eor Potential of Gas and Water Injection in Shale Oil Reservoirs. *J. Unconv. Oil and Gas Res.* **2014**, *5*, 1-9.
16. Sheng, J. J. Critical Review of Field Eor Projects in Shale and Tight Reservoirs. *J. Petrol. Sci. and Eng.* **2017**, *159*, 654-665.
17. Sun, H.; Zhao, H.; Qi, N.; Li, Y. Effects of Surface Composition on the Microbehaviors of Ch4 and CO_2 in Slit-Nanopores: A Simulation Exploration. *ACS Omega* **2017**, *2*, 7600-7608.
18. Wang, S.; Javadpour, F.; Feng, Q. Fast Mass Transport of Oil and Supercritical Carbon Dioxide through Organic Nanopores in Shale. *Fuel* **2016**, *181*, 741-758.
19. Zhang, H.; Cao, D. Molecular Simulation of Displacement of Shale Gas by Carbon Dioxide at Different Geological Depths. *Chem. Eng. Sci.* **2016**, *156*, 121-127.

20. Sun, H.; Zhao, H.; Qi, N.; Qi, X.; Zhang, K.; Li, Y. Molecular Insight into the Micro-Behaviors of CH_4 and CO_2 in Montmorillonite Slit-Nanopores. *Mol. Simul.* **2017**, *43*, 1004-1011.
21. Santos, M. S.; Franco, L. F.; Castier, M.; Economou, I. G. Molecular Dynamics Simulation of N-Alkanes and CO_2 Confined by Calcite Nanopores. *Energy Fuels* **2018**, *32*, 1934-1941.
22. Wang, R.; Peng, F.; Song, K.; Feng, G.; Guo, Z. Molecular Dynamics Study of Interfacial Properties in CO_2 Enhanced Oil Recovery. *Fluid Phase Equilibr.* **2018**, *467*, 25-32.
23. Pu, J.; Qin, X.; Gou, F.; Fang, W.; Peng, F.; Wang, R.; Guo, Z. Molecular Modeling of CO_2 and N-Octane in Solubility Process and A-Quartz Nanoslit. *Energies* **2018**, *11*, 3045.
24. Le, T.; Striolo, A.; Cole, D. R. CO_2–C_4H_{10} Mixtures Simulated in Silica Slit Pores: Relation between Structure and Dynamics. *J. Phys. Chem. C* **2015**, *119*, 15274-15284.
25. Sun, H.; Zhao, H.; Qi, N.; Qi, X.; Zhang, K.; Sun, W.; Li, Y. Mechanistic Insight into the Displacement of CH_4 by CO_2 in Calcite Slit Nanopores: The Effect of Competitive Adsorption. *RSC Advances* **2016**, *6*, 104456-104462.
26. Le, T.; Ogbe, S.; Striolo, A.; Cole, D. R. N-Octane Diffusivity Enhancement Via Carbon Dioxide in Silica Slit-Shaped Nanopores–a Molecular Dynamics Simulation. *Mol. Simul.* **2016**, *42*, 745-752.
27. Liu, B.; Shi, J.; Sun, B.; Shen, Y.; Zhang, J.; Chen, X.; Wang, M. Molecular Dynamics Simulation on Volume Swelling of CO_2–Alkane System. *Fuel* **2015**, *143*, 194-201.
28. Zhang, J.; Pan, Z.; Liu, K.; Burke, N. Molecular Simulation of CO_2 Solubility and Its Effect on Octane Swelling. *Energy Fuels* **2013**, *27*, 2741-2747.
29. Zheng, S.; Li, H. A.; Sun, H.; Yang, D. Determination of Diffusion Coefficient for Alkane Solvent–CO_2 Mixtures in Heavy Oil with Consideration of Swelling Effect. *Ind. Eng. Chem. Res.* **2016**, *55*, 1533-1549.
30. Jin, L.; Hawthorne, S.; Sorensen, J.; Pekot, L.; Kurz, B.; Smith, S.; Heebink, L.; Herdegen, V.; Bosshart, N.; Torres, J. Advancing CO_2 Enhanced Oil Recovery and Storage in Unconventional Oil Play—Experimental Studies on Bakken Shales. *Appl. Energ.* **2017**, *208*, 171-183.
31. Eide, O.; Ersland, G.; Brattekas, B.; Haugen, A.; Graue, A.; Ferno, M. CO_2 EOR by Diffusive Mixing in Fractured Reservoirs. *Petrophysics* **2015**, *56*, 23-31.
32. Lwisa, E. G.; Abdulkhalek, A. R. In *Enhanced Oil Recovery by Nitrogen and Carbon Dioxide Injection Followed by Low Salinity Water Flooding for Tight Carbonate Reservoir: Experimental Approach*, IOP Conference Series: Materials Science and Engineering, IOP Publishing: 2018; p 012009.
33. Eide, Ø.; Fernø, M. A.; Alcorn, Z.; Graue, A. Visualization of Carbon Dioxide Enhanced Oil Recovery by Diffusion in Fractured Chalk. *SPE J.* **2016**, *21*, 112-120.
34. Khan, C.; Amin, R.; Madden, G. Effects of CO_2 and Acid Gas Injection on Enhanced Gas Recovery and Storage. *J. Petrol. Explor. Prod. Technol.* **2013**, *3*, 55-60.
35. Huerta, M. M.; Alvarez, J. M.; Jossy, E.; Forshner, K. In *Use of Acid Gas (CO_2/H_2S) for the Cyclic Solvent Injection (Csi) Process for Heavy Oil Reservoirs*, SPE Heavy Oil Conference Canada, Society of Petroleum Engineers: 2012.
36. Chialvo, A. A.; Vlcek, L.; Cole, D. R. Acid Gases in CO_2-Rich Subsurface Geologic Environments. *Rev. Mineral. Geochem.* **2013**, *77*, 361-398.
37. Badmos, S.; Striolo, A.; Cole, D. R. Aqueous Hydrogen Sulphide in Slit-Shaped Silica Nano-Pores: Confinement Effects on Solubility, Structural and Dynamical Properties. *J. Phys. Chem. C* **2018**.
38. Rother, G.; Krukowski, E. G.; Wallacher, D.; Grimm, N.; Bodnar, R. J.; Cole, D. R. Pore Size Effects on the Sorption of Supercritical CO_2 in Mesoporous Cpg-10 Silica. *J. Phys. Chem. C* **2011**, *116*, 917-922.
39. Causa, M.; Dovesi, R.; Pisani, C.; Roetti, C. Ab Initio Hartree-Fock Study of the MgO (001) Surface. *Surf. Sci.* **1986**, *175*, 551-560.

40. Scamehorn, C.; Hess, A.; McCarthy, M. Correlation Corrected Periodic Hartree–Fock Study of the Interactions between Water and the (001) Magnesium Oxide Surface. *J. Chem. Phys.* **1993**, *99*, 2786-2795.
41. Ho, T. A.; Striolo, A. Water and Methane in Shale Rocks: Flow Pattern Effects on Fluid Transport and Pore Structure. *AIChE J.* **2015**, *61*, 2993-2999.
42. Teich-McGoldrick, S. L.; Greathouse, J. A.; Cygan, R. T. Molecular Dynamics Simulations of Structural and Mechanical Properties of Muscovite: Pressure and Temperature Effects. *J. Phys. Chem. C* **2012**, *116*, 15099-15107.
43. Wang, J.; Kalinichev, A. G.; Kirkpatrick, R. J.; Cygan, R. T. Structure, Energetics, and Dynamics of Water Adsorbed on the Muscovite (001) Surface: A Molecular Dynamics Simulation. *J. Phys. Chem. B* **2005**, *109*, 15893-15905.
44. White, W. M. *Geochemistry*; John Wiley & Sons, 2013.
45. Tuladhar, A.; Chase, Z. A.; Baer, M. D.; Legg, B. A.; Tao, J.; Zhang, S.; Winkelman, A. D.; Wang, Z.; Mundy, C. J.; De Yoreo, J. J. Direct Observation of the Orientational Anisotropy of Buried Hydroxyl Groups inside Muscovite Mica. *J. Am. Chem. Soc.* **2019**, *141*, 2135-2142.
46. Sakuma, H.; Kawamura, K. Structure and Dynamics of Water on Li+-, Na+-, K+-, Cs+-, H_3O+-Exchanged Muscovite Surfaces: A Molecular Dynamics Study. *Geochim. Cosmochim. Acta* **2011**, *75*, 63-81.
47. Sakuma, H.; Kawamura, K. Structure and Dynamics of Water on Muscovite Mica Surfaces. *Geochim. Cosmochim. Acta* **2009**, *73*, 4100-4110.
48. Cygan, R. T.; Liang, J.-J.; Kalinichev, A. G. Molecular Models of Hydroxide, Oxyhydroxide, and Clay Phases and the Development of a General Force Field. *J. Phys. Chem. B* **2004**, *108*, 1255-1266.
49. Martin, M. G.; Siepmann, J. I. Transferable Potentials for Phase Equilibria. 1. United-Atom Description of N-Alkanes. *J. Phys. Chem. B* **1998**, *102*, 2569-2577.
50. Kamath, G.; Potoff, J. J. Monte Carlo Predictions for the Phase Behavior of H_2S+N-Alkane, H_2S+ CO_2, CO_2+ CH_4 and H_2S+ CO_2+ CH_4 Mixtures. *Fluid Phase Equilibr.* **2006**, *246*, 71-78.
51. Coasne, B.; Galarneau, A.; Di Renzo, F.; Pellenq, R. Molecular Simulation of Nitrogen Adsorption in Nanoporous Silica. *Langmuir* **2010**, *26*, 10872-10881.
52. Allen, M. P.; Tildesley, D. J. *Computer Simulation of Liquids*; Oxford University Press: Oxford, UK, 2004.
53. Essmann, U.; Perera, L.; Berkowitz, M. L.; Darden, T.; Lee, H.; Pedersen, L. G. A Smooth Particle Mesh Ewald Method. *J. Chem. Phys.* **1995**, *103*, 8577-8593.
54. Van Der Spoel, D.; Lindahl, E.; Hess, B.; Groenhof, G.; Mark, A. E.; Berendsen, H. J. C. Gromacs: Fast, Flexible, and Free. *J. Comput. Chem.* **2005**, *26*, 1701-1718.
55. Abraham, M. J.; Murtola, T.; Schulz, R.; Páll, S.; Smith, J. C.; Hess, B.; Lindahl, E. Gromacs: High Performance Molecular Simulations through Multi-Level Parallelism from Laptops to Supercomputers. *SoftwareX* **2015**, *1*, 19-25.
56. Song, Y.; Dai, L. L. The Shear Viscosities of Common Water Models by Non-Equilibrium Molecular Dynamics Simulations. *Mol. Simul.* **2010**, *36*, 560-567.
57. Sun, H.; Zhao, H.; Qi, N.; Li, Y. Simulation to Enhance Shale Gas Recovery Using Carbon Dioxide in Silica Nanopores with Different Sizes. *Energy Technol.* **2017**, *5*, 2065-2071.
58. Kinaci, A.; Haskins, J. B.; Çağın, T. On Calculation of Thermal Conductivity from Einstein Relation in Equilibrium Molecular Dynamics. *J. Chem. Phys.* **2012**, *137*, 014106.
59. Kadoura, A.; Narayanan Nair, A. K.; Sun, S. Molecular Dynamics Simulations of Carbon Dioxide, Methane, and Their Mixture in Montmorillonite Clay Hydrates. *J. Phys. Chem. C* **2016**, *120*, 12517-12529.

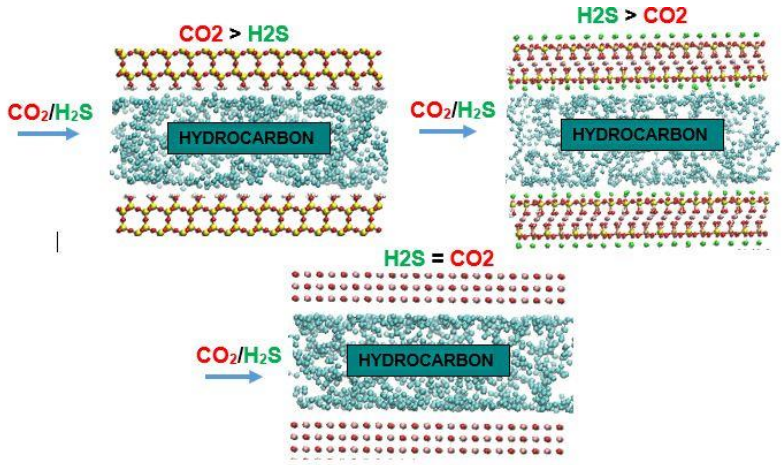

Graphic for the Table of Contents